Shapes and shape transformations of two-component membranes of complex topology

Wojciech T. Góźdź* and Gerhard Gompper
Max-Planck-Institut für Kolloid und Grenzflächenforschung, Kantstrasse 55, 14513 Teltow, Germany
(Received 1 October 1998)

The properties of two-component membranes, which form doubly periodic surfaces of complex topology, are studied in the strong-segregation limit. The membrane is described within the framework of curvature elasticity; the two components are distinguished by their spontaneous curvatures in this case. Four different domain morphologies are considered for a square lattice of passages: rings of component α inside the passage and caplets of component α outside the passage, as well as rings and caplets of component β. The dependences of the shape of the membrane and of the shape of the domain boundary are calculated as a function of composition. On the basis of a calculation of the curvature energy we conjecture the existence of doubly periodic, piecewise constant-mean-curvature surfaces. For small and intermediate line tensions, we predict several phase transitions between the investigated morphologies. We also discuss briefly the existence and shapes of vesicles of piecewise constant mean curvature. [S1063-651X(99)02304-1]

PACS number(s): 64.60.−i, 68.10.Cr, 87.16.Dg

I. INTRODUCTION

Membranes made of amphiphilic molecules are present in many soft-matter systems [1,2]. Typical examples are surfactant monolayers, which assemble at the oil-water interface or at the water-air interface in ternary amphiphilic systems, and lipid bilayers, which form the walls of all biological cells. Biological membranes are not homogeneous, but consist of many different components [3,4]. These components are several species of lipids, but also include many kinds of membrane proteins. In order to understand the role of the various components in biological membranes, model systems have been developed for studying pure lipids, lipid mixtures, and reconstituted lipid-protein mixtures.

The presence of several components in a membrane leads to the possibility of lateral phase separation. The molecules demix and form domains, in which one or more components are enriched. Two-component mixtures have been studied experimentally in considerable detail for monolayers at the air-water interface. In particular, mixtures of phospholipids and cholesterol show clear fluid-fluid coexistence [5,6], and phase diagrams have been determined [7]. The case of two-component bilayers is more complicated. Although there is strong evidence for cluster formation on small length scales [8,9], the evidence for macroscopic phase separation is still rather indirect [10–15]. Fluid-fluid coexistence could also occur between a protein-rich and a protein-poor phase of membrane proteins embedded in a homogeneous amphiphile layer [16,17]; a similar two-phase coexistence may be found in mixtures of lipids and polymers with lipid anchors [18,19].

Since the composition and shape of a membrane are coupled locally, phase separation leads to domain-induced shape changes or shape transitions. The effect of phase separation on the shapes of almost planar membranes [20–22] and of vesicles of spherical topology [23–27] has been studied theoretically in some detail. Again, monolayers and bilayers have to be distinguished. In the former case, the composition couples linearly to the preferred, ''spontaneous'' curvature of the monolayer. In the latter case, the situation is more complicated, because the compositions of both leaves of the bilayer determine its spontaneous curvature. The situation simplifies, for example, if the domain structure in the upper leave is anticorrelated with the domain structure in the lower leave, or if the bilayer is strongly asymmetric, so that one leave consists only of a single component. In these cases, the bilayer can be described by the same model as employed for monolayers.

In this paper, we study the effect of phase separation in a more complex topology, in which two membranes are connected by a lattice of passages. For homogeneous membranes, this type of topology has been observed in ''catenoid'' lamellar phases [28–30] of block-copolymer mixtures and in multilamellar vesicles of phospholipid membranes [31,32].

It is important to note that phase separation and domain-induced shape transformation strongly affect the functions of biomembranes [3,33,21,8,9]. Here, a change of the membrane composition seems to be a very effective way of varying membrane shape. This change in composition is not necessarily due to an exchange of molecules, but can be often more easily achieved by an adsorption of polymers or proteins, which change the local spontaneous curvature of the membrane. A well-known example for such a process is the formation of vesicles after adsorption of a clathrin coat onto a planar membrane [34].

II. MODEL FOR TWO-COMPONENT MEMBRANES

The system we investigate is a fluid membrane composed of two different types of molecules, which have a strong tendency towards phase separation. The membrane forms a square lattice of passages of lattice constant L; see Fig. 1. This is the same topology which is found in the doubly periodic surfaces of constant mean curvature, which were first studied by Lawson [35]. Indeed, in the limit of a single-

*Permanent address: Institute of Physical Chemistry, Polish Academy of Sciences and College of Science, Kasprzaka 44/52, 01-224 Warsaw, Poland.

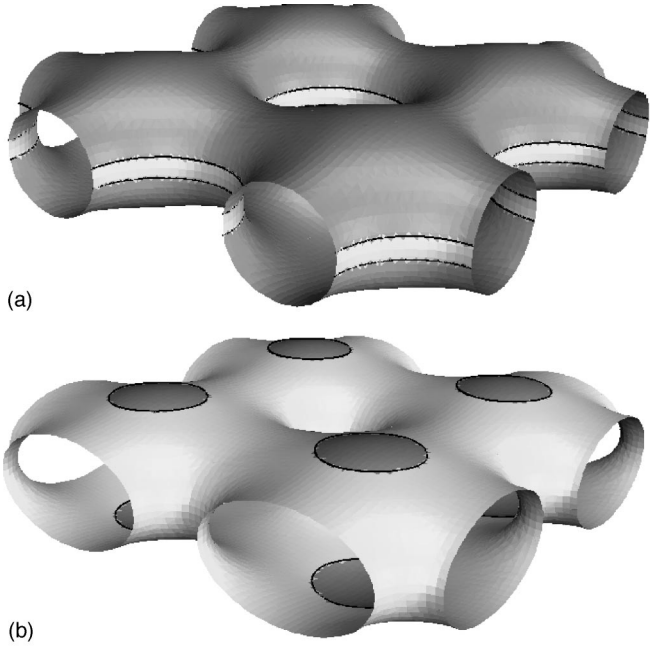

FIG. 1. Lattice of passages with different domain morphologies: (a) (inverted) ring morphology ($\phi=0.932$), (b) (inverted) caplet morphology ($\phi=0.113$). The spontaneous curvatures of the two components are $Lh_0^{(\alpha)}=1.2$ (dark) and $Lh_0^{(\beta)}=0.4$ (light), respectively; the scaled line tension is $\lambda L/\kappa=10^{-4}$.

component membrane, our membranes take the shape of the Lawson surface. The molecules can demix and form coherent domains of one component with well-defined boundaries. We consider two types of domains. A domain may be located inside a passage, forming a ring around the passage; see Fig. 1(a). We call this a ''ring'' configuration. A domain may be also located outside a passage, in the regions of the membrane which are approximately parallel to the midplane between its upper and lower leaves, forming a roughly circular caplet; see Fig. 1(b). We call this a ''caplet'' configuration. The caplet configuration is analogous to droplet phases observed in bulk liquids (except that the space dimension is 2 rather than 3).

At sufficiently low temperatures, the phase-separated domains consist almost exclusively of a single component, and the interface between the domains is very sharp. This is the strong-segregation limit we want to investigate in this paper, since the effect of phase separation on the membrane shape is most pronounced in this case. The strong-segregation limit has been investigated in Refs. [23,24,26] for vesicles and in Ref. [22] for almost planar membranes [36]. At higher temperatures, the components begin to mix inside the domains, until the two-phase coexistence vanishes in a critical point.

The molecules composing the mixture are characterized by the tendency to form membranes of locally constant mean curvature. This behavior is modelled by coupling the local composition to the local mean curvature. In the limit of large radii of curvature (compared to the thickness), the membrane can then be approximated by an infinitely thin ''mathematical'' surface with its shape determined by the curvature energy

$$\mathcal{H}=\kappa\int_S d^2\sigma\sqrt{g(\sigma)}[H(\sigma)-H_0(\sigma|S^{(\alpha)},S^{(\beta)})]^2 + \lambda\oint_{\partial S^{(\alpha)}} dl, \tag{1}$$

where $\sigma=(\sigma^1,\sigma^2)$ defines the internal coordinate system of the membrane, and $\mathbf{R}(\sigma)$ describes the position of a membrane element in the embedding space. In Eq. (1), $g(\sigma)$ is the determinant of the metric tensor $g_{ij}(\sigma)=\partial\mathbf{R}(\sigma)/\partial\sigma^i\cdot\partial\mathbf{R}(\sigma)/\partial\sigma^j$, and $H(\sigma)$ the local mean curvature. κ denotes the bending rigidity and λ is the line tension of the domain boundary. The local spontaneous curvature $H_0(\sigma|S^{(\alpha)},S^{(\beta)})$ depends on the domain structure on the membrane; it is constant within each domain of α and β components, with $H_0(\sigma|S^{(\alpha)},S^{(\beta)})=h_0^{(\gamma)}$ for all points on the surface which are part of $S^{(\gamma)}$, where $\gamma\in\{\alpha,\beta\}$.

For simplicity, the bending rigidity κ and the Gaussian rigidity κ_G are assumed to be independent of the local composition. Since the curvature energy (1) forces the mean curvature to be smooth at the domain boundary [37], a Gaussian-curvature term in the Hamiltonian would contribute a constant to the energy, according to the Gauss-Bonnet theorem for periodic surfaces; such a term is therefore omitted here. The line-tension integral is taken along the boundary which separates different components of the membrane.

The basic length and energy scales for the problem are set by the lattice constant L and the bending rigidity κ. It is important to note that no surface-tension term appears in Eq. (1), so that the area of the membrane (and also the enclosed volume) is not constrained.

III. NUMERICAL METHODS

In order to describe the membrane shape in the case of a complex topology, we use the implicit representation

$$\omega(x,y,z)=1-B(x,y)Q(z)=0, \tag{2}$$

where $Q(z)\geqslant 0$ is a symmetric ''weight function,'' which equals unity at $z=0$, decays strictly monotonically with increasing $|z|$, and vanishes in the limit of large $|z|$. This ansatz can be most easily understood by identifying $\omega(x,y,z)$ with the concentration difference of oil and water in a ternary system, and the membrane with an amphiphilic monolayer. Then, $\omega(x,y,z)>0$ on one side of the membrane (the ''oil side'') and $\omega(x,y,z)<0$ on the other side (the ''water side''). For a point (x,y) in the midplane with $B(x,y)<1$, $\omega(x,y,z)>0$ for all z, so that there is no membrane present; such a point is located inside the ''oil channel'' through the passage. For a point with $B(x,y)>1$, on the other hand, $\omega(x,y,z)<0$ for small $|z|$, but $\omega(x,y,z)>0$ for large $|z|$. The choice of the weight function in Eq. (2) is arbitrary, and does not affect the shape of the membrane after minimization. We take $Q(z)=1/\cosh^2(z)$, so that the membrane is located at

$$\cosh(z)=\sqrt{B(x,y)}. \tag{3}$$

Our choice of the weight function is motivated by the form of the equation for the catenoid minimal surface, which is

recovered from Eq. (3) for $B(x,y)=x^2+y^2$. The membrane is symmetric with respect to the $z=0$ plane by construction.

For surfaces described by the Monge representation (3), with $\sigma=(x,y)$ and $\mathbf{R}(\sigma)=(x,y,z(x,y))$, the determinant of the metric tensor is given by $g(x,y)=\sqrt{1+|\nabla z(x,y)|^2}$, and the mean curvature is

$$2H(x,y)=\nabla\cdot\frac{\nabla z(x,y)}{\sqrt{1+|\nabla z(x,y)|^2}}. \tag{4}$$

In order to describe a square lattice of passages by Eq. (3), $B(x,y)$ is expanded into the Fourier series

$$B(x,y)=a_0+\sum_{i=1}^{N} a_i \sum_{j=1}^{N_i} \cos\left(\frac{2\pi}{L}\mathbf{k}_j^{(i)}\cdot\mathbf{r}\right), \tag{5}$$

where $\mathbf{r}=(x,y)$, N is the number of Fourier amplitudes, $\mathbf{k}_j^{(i)}$ are the reciprocal lattice vectors, and N_i is their number in the ith shell. Here, a shell is the set of reciprocal lattice vectors of the same length, which are related to each other by symmetry operations characteristic for a given lattice. No $\sin[(2\pi/L)\mathbf{k}_j^{(i)}\cdot\mathbf{r}]$ terms appear in the expansion (5) because we assume the full symmetry of the square lattice. We want to emphasize that such a choice for $B(x,y)$ makes the membrane smooth at the unit cell boundaries by construction.

The shape of the domain boundary is written in cylindrical coordinates (ρ,θ,z) as

$$\rho(\theta)=\rho_0+\sum_{i=1}^{N_\rho}\rho_i\cos(4i\theta),$$

$$z=\cosh^{-1}[\sqrt{B(\rho(\theta)\cos(\theta),\rho(\theta)\sin(\theta))}], \tag{6}$$

where the coefficients ρ_i for $i=0,\ldots,N_\rho$ describe the local radius of the domain boundary. Such a parametrization guarantees that the domain boundaries have fourfold symmetry. The origin of cylindrical coordinates is located either at the middle (for ring morphology) or at the corner (for caplet morphology) of the unit cell; compare Fig. 1.

With the parametrization of the membrane and domain-boundary shapes given by Eqs. (5) and (6), the functional (1) is minimized with respect to the coefficients a_i and ρ_i under the constraint of constant composition $\phi=S^{(\alpha)}/(S^{(\alpha)}+S^{(\beta)})$; i.e., the ratio of the surface areas occupied by the two components is kept constant during the minimization. The topology of the membrane is not allowed to change with composition. The number of coefficients ρ_i is always the same and equal to 5. Although it is sufficient to use a few coefficients a_i to obtain good approximation of global properties (like total surface area, domain-boundary length, and radius of the passage at $z=0$), the accurate calculation of the local properties of the membrane (like the local mean curvature and thus the curvature energy) requires N to be large. We have performed calculations for 32, 49, 66, and 89 coefficients a_i. These numbers are chosen to include all shells with reciprocal lattice vectors of lengths less or equal to 8, 10, 12, and 14 (in the units of $2\pi/L$), respectively.

IV. RESULTS

A. Lattice of passages for one-component membranes

The existence of doubly periodic surfaces of constant mean curvature was proved by Lawson [35] almost 30 years ago, but their properties have not been studied in much detail so far [38]. As a result of the periodicity, the integral of the Gaussian curvature within a unit cell is constant and equal to -4π. Thus the Euler characteristics $\chi=\int_S K dS/2\pi$ and genus $g=(2-\chi)/2$ are appropriately -2 and 2 for this family of constant-mean-curvature (CMC) surfaces.

The results of our numerical calculations done with the curvature energy (1) with $h_0^{(\alpha)}=h_0^{(\beta)}=h_0$ and $\lambda=0$ agree very well with the exact predictions. The integral $\int_S(H-h_0)^2dS$ already vanishes within the numerical accuracy for 31 Fourier modes in the Fourier expansion (5), indicating that the proposed parametrization works remarkably well for one-component membranes. Surface shapes obtained with our parametrization (3) and (5) are shown in Fig. 2.

For small mean curvature, the surface shape resembles two planes, which are connected by a square lattice of narrow passages; compare Fig. 2(a). The passage radius and the planes separation become smaller and smaller with decreasing mean curvature, and finally merge into a single plane for $Lh_0=0$. When the mean curvature is increased the membrane ultimately deforms into a square lattice of touching spheres at $Lh_0=2$. However, this transformation into touching spheres is quite complicated. For $Lh_0\nearrow 2$, a membrane shape is obtained, which is different from touching spheres. This shape develops smoothly as the spontaneous curvature increases to $Lh_0\simeq 2.3$; compare Figs. 3 and 4. Therefore, there must be a second branch of CMC surfaces, along which this shape of maximum Lh_0 transforms into touching spheres. This behavior is, in fact, very similar to the behavior observed for triply periodic CMC surfaces in the limit of ''large'' Lh_0 [39]. The quality of the parametrization (3), (5) for the extremal values of the mean curvature decreases due to the difficulty in describing very narrow necks (which appear in both limits) with a limited number of amplitudes in the Fourier expansion.

The properties of the doubly periodic Lawson surface can be characterized quantitatively by the volume and surface area per unit cell, and by the (orientation-dependent) radius of the passage in the $z=0$ plane. The results for different mean curvatures in the range $0.2\leqslant Lh_0\leqslant 2.3$ are shown in Figs. 3 and 4. The volume per unit cell, the surface area, and the radius of the passage are all found to be *nonmonotonic* functions of Lh_0. Another interesting quantity is the passage shape in the $z=0$ plane. For the range of mean curvatures $0<Lh_0\leqslant 1.2$, the passage is almost exactly circular; it begins to deviate appreciably from a circle for higher mean curvatures; see Fig. 3.

In our study of two-component membranes we have chosen the spontaneous curvatures $Lh_0^{(\alpha)}=1.2$ and $Lh_0^{(\beta)}=0.4$ for each component; these spontaneous curvatures are significantly different, but not too close to the extremal values of Lh_0. The shapes of constant-mean-curvatures surfaces characterized by these two values of Lh_0 are shown in Fig. 2.

B. Role of a line tension

The behavior of periodic one-component membranes, which do not change their topology, is totally governed by

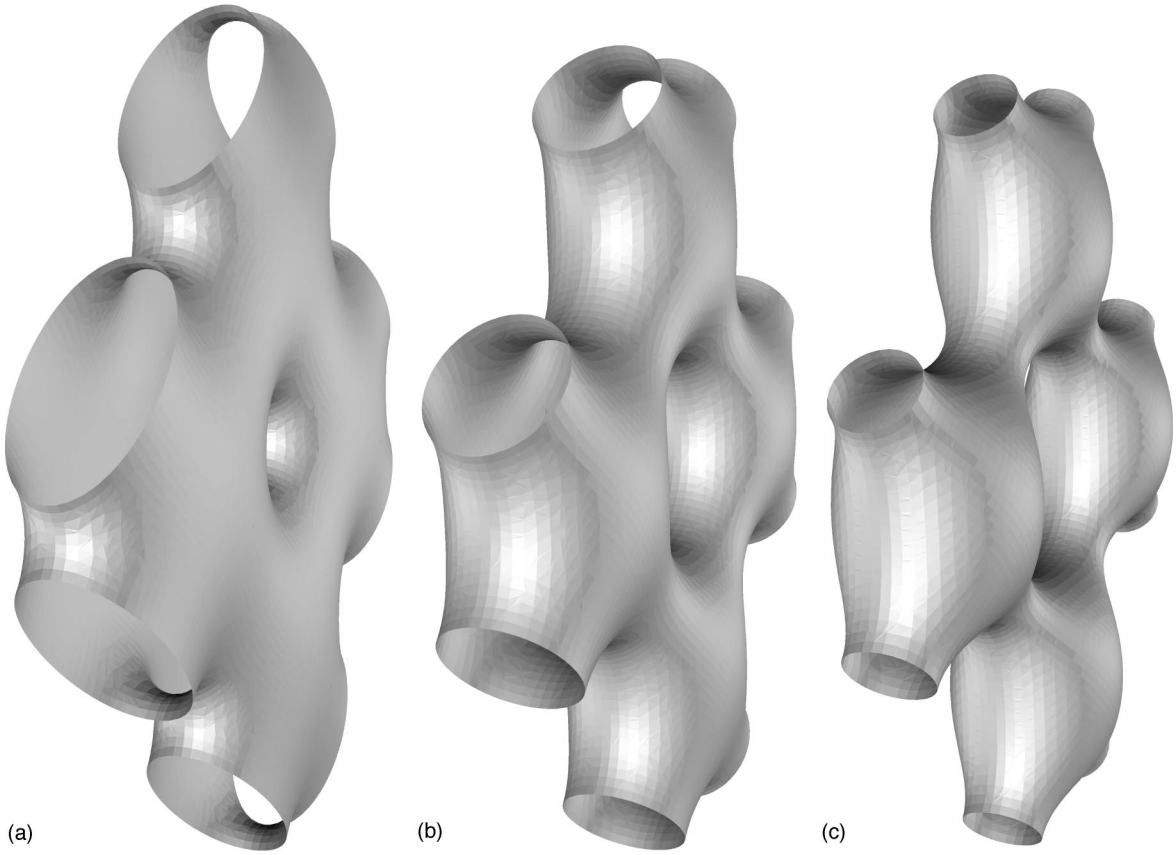

FIG. 2. Shapes of one-component membranes for different spontaneous curvatures. (a) $Lh_0=0.4$, (b) $Lh_0=1.2$, (c) $Lh_0=1.9$. $N=49$ Fourier shells have been used in the expansion (5).

the bending energy. For two-component membranes the line tension begins to play an important role and the membrane shape is the result of competition between the bending energy and line tension. For line tensions which are ''large'' compared to the curvature energy, the membrane adapts a shape which reduces the length ℓ of the domain boundary at the cost of the curvature energy. If the line tension is sufficiently large, the boundary length will shrink to zero, which causes budding of the domains (in the caplet morphology) [21]. On the other hand, when the line tension is small com-

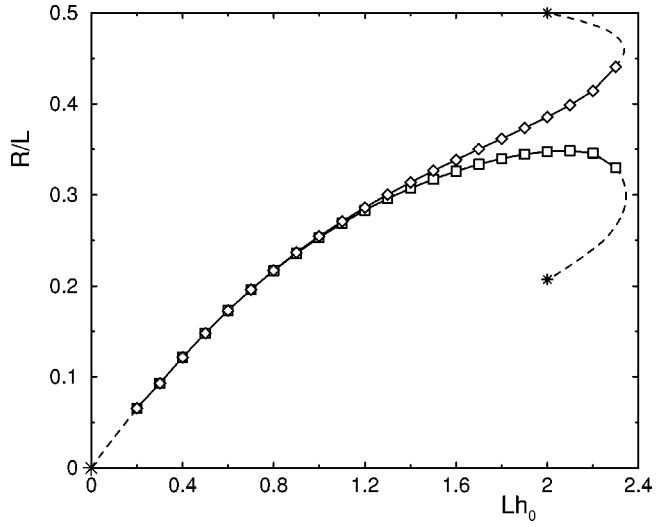

FIG. 3. Passage radii in the $z=0$ plane for one-component membranes as a function of the scaled spontaneous curvature Lh_0. Circles (○) represent the passage radius along the (10), squares (□) along the (11) direction. The stars denote the limiting values for $Lh_0=0.0$ (plane) and $Lh_0=2.0$ (touching spheres). The dotted lines show plausible interpolations between the calculated data (for $N=49$ Fourier shells) and the limiting shapes.

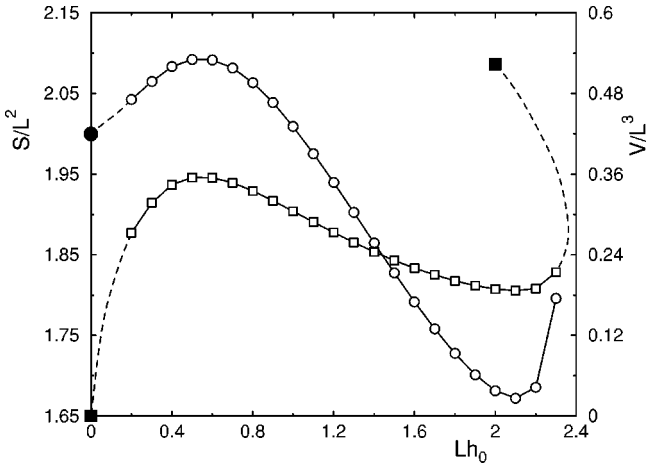

FIG. 4. Surface area (○) and volume (□) of a unit cell for one-component membranes as a function of the scaled spontaneous curvature Lh_0. The solid square (■) and circle (●) denote the limiting values for $Lh_0=0.0$ (plane) and $Lh_0=2.0$ (touching spheres). The value of the surface area for touching spheres is $\pi=3.1415\ldots$ and is not shown. $N=49$ shells have been used in the Fourier expansion.

pared to the curvature energy, the membrane adapts the best shape to minimize the curvature energy at the cost of the length of the domain boundaries. In the weak-line-tension limit the membrane shape is mainly determined by the bending energy, similarly as in the case of one-component membranes.

We have investigated both regimes of weak and strong line tension, with the main focus on the limit of weak line tensions. In order to estimate the borderline between these two regimes, we have performed calculations for different $L\lambda/\kappa$, increasing $\lambda L/\kappa$ in each step by an order of magnitude from $\lambda L/\kappa = 10^{-4}$ to $\lambda L/\kappa = 10$. The line tension begins to influence the membrane properties for $\lambda L/\kappa \geqslant 10^{-1}$ and becomes significant for $\lambda L/\kappa = 1$. A line tension of the order of $\lambda L/\kappa = 10$ already leads to budding for caplet morphologies. For example, the passage radius for the ring morphology with $\phi = 0.1$ changes from $R/L = 0.132$ for $\lambda L/\kappa < 10^{-2}$ to $R/L = 0.123$ for $\lambda L/\kappa = 10^{-1}$ and $R/L = 0.085$ for $\lambda L/\kappa = 1.0$. The effect of the line tension is weaker for larger values of ϕ; compare Sec. IV G below. Other properties like surface area S and domain perimeter ℓ behave similarly.

Finally, we have considered membranes with *constant* spontaneous curvature, i.e., $Lh_0^{(\alpha)} = Lh_0^{(\beta)} = Lh_0$, and the line tension $\lambda L/\kappa = 10^{-4}$, with the domain boundaries located in the $z = 0$ plane. This corresponds to two-component membranes (in the limit $\phi \to 0$), where both components have the same spontaneous curvature, but do not mix. The curvature energy is found to change from $E_b/\kappa = 6.97 \times 10^{-9}$ (for $\lambda L/\kappa = 0$) to $E_b/\kappa = 7.31 \times 10^{-9}$ for $N = 49$ and $Lh_0 = 0.4$. Based on these calculation we decided to use $\lambda L/\kappa = 10^{-4}$ in weak-line-tension limit and $\lambda L/\kappa = 1$ for the case of a large line tension.

C. Shapes of two-component membranes: Weak line tensions

Each of the two components can form closed domains within a membrane composed of the other component. Since we consider two domains morphologies (rings [see Fig. 1(a)] and caplets [see Fig. 1(b)]), there are four possible configurations of domains in the membrane.

Naively one might expect that the component coupled to the smaller spontaneous curvature preferentially occupies the flatter parts and the component coupled to the higher curvature the more strongly curved parts (in the neck of the passage) of the membrane. Thus, two configurations should be favored, namely, when component α (with $Lh_0^{(\alpha)} = 1.2$) forms rings or component β (with $Lh_0^{(\beta)} = 0.4$) forms caplets. We call these two configurations ''caplets'' and ''rings,'' respectively, while the other two (where component α forms caplets and component β forms rings) are denoted ''inverted caplets'' and ''inverted rings.'' Surprisingly, it turns out that for the studied topology the location of domains is not determined by the curvature energy, because the membrane can equally adapt an optimal shape for any of these four configurations.

It is convenient to examine the membrane properties as a function of composition ϕ, since $\phi = S^{(\alpha)}/(S^{(\alpha)} + S^{(\beta)})$ is well defined and easily accessible in experiments. When the composition decreases to zero, for caplet morphologies the domain degenerates into a point, the boundary length ℓ vanishes, and membrane shape approaches the shape of a homogeneous membrane discussed in Sec. IV A. In the case of ring morphologies, on the other hand, ℓ approaches the length of the neck perimeter in the $z = 0$ plane, still causing a deformation of the membrane (depending, of course, on the value of the line tension).

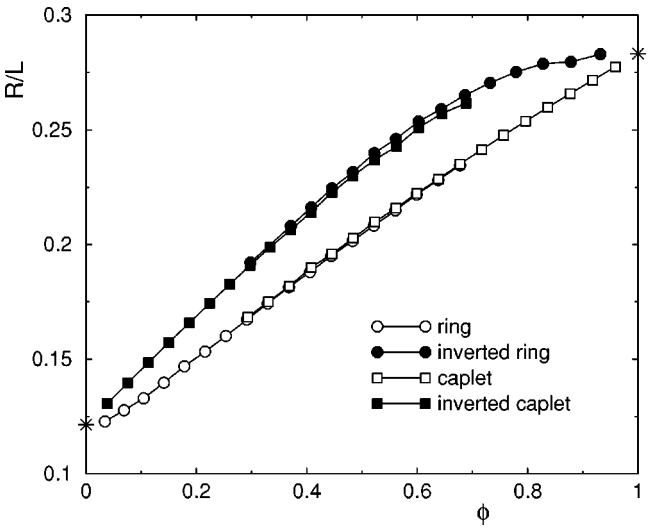

FIG. 5. Passage radius in the $z = 0$ plane for different morphologies of two-component membranes as a function of composition ϕ (for $N = 49$ Fourier shells). The stars denote the values for pure membranes, with $Lh_0^{(\alpha)} = 1.2$ and $Lh_0^{(\beta)} = 0.4$. The scaled line tension is $\lambda L/\kappa = 10^{-4}$.

For two-component membranes with $Lh_0^{(\alpha)} = 1.2$ and $Lh_0^{(\beta)} = 0.4$, within the whole range of compositions and for all types of configurations, the passage shape in the $z = 0$ symmetry plane is almost ideally circular, similarly as it is for pure membranes. While for one-component membranes the passage radius varies with the mean curvature, for two-component membranes it varies with composition. It turns out that even a small amount of the second component causes the shape to change. For all configurations, the passage radius increases monotonically with composition ϕ, approaching the values characteristic for pure membranes for $\phi \to 0$ or $\phi \to 1$; this indicates that the line tension $L\lambda/\kappa = 10^{-4}$ indeed does not influence the membrane shape; compare Fig. 5. It is quite unexpected that for ring and caplet morphologies, the radius is almost the same for the same composition ϕ, and is roughly proportional to the composition. One might expect that the location of a domain inside the passage would have a stronger effect on its radius than its location in the membrane segments with positive Gaussian curvature, since it seems to be easier to deform the passage than the ''flat'' parts of the membrane. However, we observe that for the same composition, caplet and ring morphologies — and similarly inverted caplet and inverted ring morphologies — show only very small differences in the size of the passage radius.

It is interesting to note that two different mechanisms have very similar effects on the passage radius. It can be varied either by changing the spontaneous curvature of a one-component membrane or by changing the composition of a two-component membrane.

The surface area of the membrane behaves similarly as the passage radius. Figure 6 shows the surface area divided

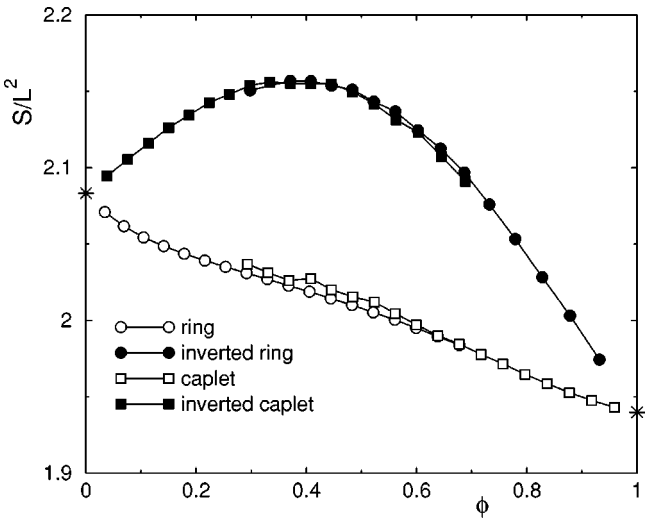

FIG. 6. Surface area for different morphologies of two-component membranes as a function of composition ϕ (for $N=49$ Fourier shells). The stars denote the values for pure membranes, with $Lh_0^{(\alpha)}=1.2$ and $Lh_0^{(\beta)}=0.4$. The scaled line tension is $\lambda L/\kappa=10^{-4}$.

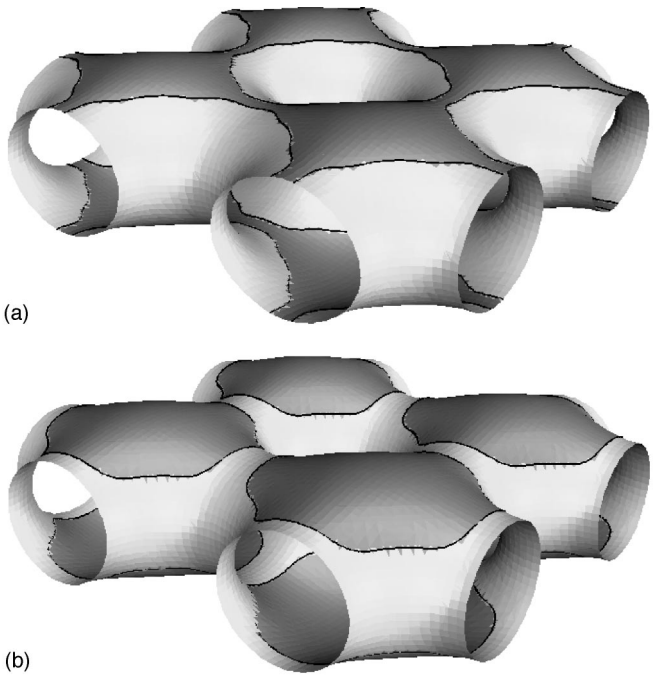

FIG. 7. Shapes of two-component membranes, which show the deformation of the domain boundary for large domains: (a) inverted ring morphology ($\phi=0.563$), (b) inverted caplet morphology ($\phi=0.371$). The spontaneous curvatures of the two components are $Lh_0^{(\alpha)}=1.2$ (dark) and $Lh_0^{(\beta)}=0.4$ (light), respectively; the scaled line tension is $\lambda L/\kappa=10^{-4}$.

by the lattice constant squared. For ring and caplet configurations the value of surface area changes monotonically and almost linearly between the values characteristic for the single-component membranes. The surface area differs only slightly for ring and caplets morphologies of the same composition. The behavior for inverted ring and inverted caplet configurations, on the other hand, is quite different and does resemble the behavior of pure membranes as a function of spontaneous curvature (compare Fig. 4); however, the nonmonotonic behavior is more pronounced here. The value of the surface area increases above the values for either one-component membrane, and reaches a maximum approximately at the composition $\phi\simeq 0.4$, compared to $Lh_0\simeq 0.54$ for single-component membranes. The surface area for the inverted configurations is larger than for the other two since the component outside of the passage has higher mean curvature.

The phase separation within the membrane gives it more flexibility to adapt various shapes. One may speculate that phase separation within a membrane provides a mechanism to activate biological functions if these functions depend on the membrane shape [3,33].

D. Shape of the domain boundary

Unlike the surface area and passage radius, the length and shape of the domain boundaries are unique features of multicomponent membranes. For a flat membrane, the optimal shape of the domain boundary is a circle, since it minimizes its length for a given surface area. However, for ''complex'' membranes the shape of the domain boundary strongly depends on the membrane topology. There is a competition between the two processes of forming the shortest domain boundary at the cost of the curvature energy and adjusting its shape to the topology of the membrane at the cost of line energy. The presence of passages and periodicity of the membrane strongly influences the shape of the domain boundary. For ring and inverted ring morphologies, the center of the passage is also the center of the domain boundary. When it is far from the unit-cell boundary, it is almost perfectly circular. However, when it approaches the unit-cell boundary, the periodicity of the lattice enforces deviations from a circular shape. These deformations are the larger the closer the domain boundary approaches the boundaries of the unit cell; see Fig. 7(a). For caplets and inverted caplets, the shape of the domain boundary is influenced both by the unit-cell boundaries *and* by the passages; see Fig. 7(b). The closer the domain boundary approaches the inner part of a passage, the larger become the deviations from a circular shape. It is interesting to note that in the limits $\phi\to 0$ and $\phi\to 1$, metastable configurations exist, for which the minority component forms a narrow strip along the cell boundaries.

Figure 8 shows the change of length ℓ of the domain boundary as a function of composition ϕ. For each of the considered morphologies there is a range of compositions, for which it has the shortest domain boundary. With increasing ϕ, we find the sequence of inverted caplets $\rightarrow$ rings $\rightarrow$ inverted rings $\rightarrow$ caplets for the morphology of minimal domain perimeters. Here, ring and caplet morphologies have the largest ranges of stability.

E. Piecewise constant-mean-curvatures surfaces

It has been demonstrated in Sec. IV A that in the lattice-of-passages geometry a *one-component* membrane can easily adapt to a shape of constant mean curvature. For membranes, which consist of pieces of different spontaneous curvatures, the shape adjusts itself such as to minimize the curvature energy and the length of the domain boundary simultaneously. In the limit of zero line tension, this might, or might

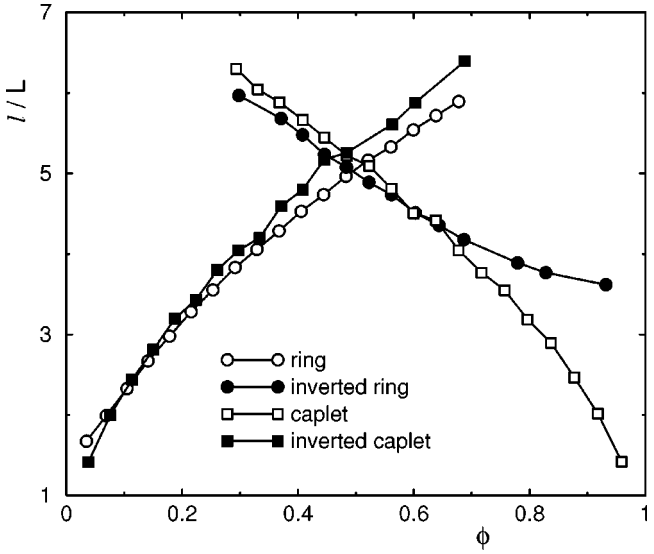

FIG. 8. Length ℓ of the domain boundaries for different morphologies as a function of composition ϕ. The parameters are the same as in Fig. 5.

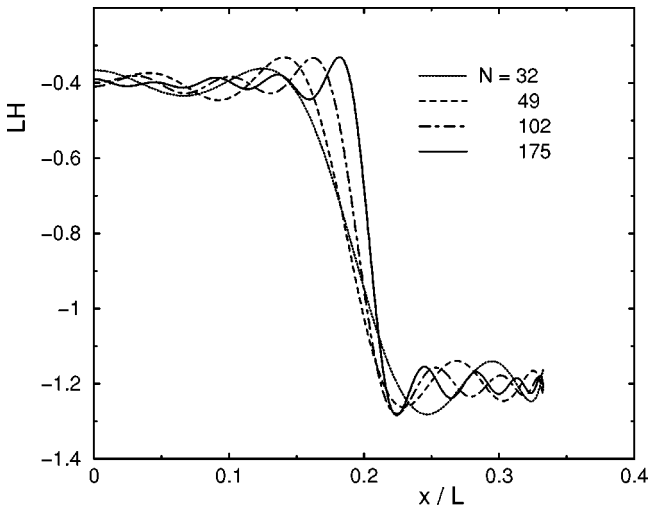

FIG. 10. Local mean curvature as a function of the distance x along a line through the center of the passage in the (10) direction. The data are obtained for the ring morphology with $\phi=0.29$ and different number of Fourier shells, as described in the text. The other parameters are the same as in Fig. 5.

not, lead to surfaces of piecewise constant mean curvature. We want to emphasize that the answer to this question is nontrivial, since the boundary conditions for the membrane pieces at the domain boundary, as discussed in Sec. II, impose strong constraints on all possible shapes.

Our data show that the free energy depends roughly linearly on the length ℓ of the domain boundary (for fixed N). This is demonstrated in Fig. 9, where we plot the (dimensionless) curvature energy — without the contribution of the line tension in Eq. (1) — per unit boundary length, $E_bL/(\kappa\ell)$. The concentration dependence of this quantity shows some oscillations around the average value, the amplitude of which decreases with increasing N. More importantly, the increase of N causes a decrease of the curvature energy. Both of these results can be attributed to the approximation of the discontinuity of the mean curvature by a Fourier series with a finite number N of Fourier modes. The decrease of $E_bL/(\kappa\ell)$ with N suggests that the energy for an infinite number of the coefficients a_i can vanish if the mean curvature of the surface behaves like a step function changing from $Lh_0^{(\alpha)}$ to $Lh_0^{(\beta)}$ along the domain boundary, and the rest of the surface is characterized by $H(\sigma)=H_0(\sigma|S^{(\alpha)},S^{(\beta)})$. A plot of the local mean curvature (see Fig. 10) supports this hypothesis, since it shows that (i) the deviation from the spontaneous curvature occurs mostly at the domain boundary, (ii) the local mean curvature remains very close to the spontaneous curvature on the rest of the membrane, and (iii) for larger N, the boundary region becomes narrower.

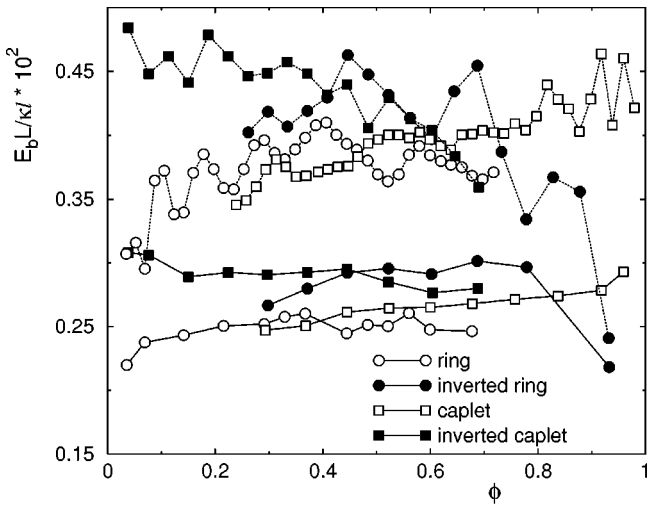

FIG. 9. Curvature energy per unit length of the domain boundary for different morphologies as a function of composition ϕ, for $N=49$ (top) and $N=66$ (bottom). The parameters are the same as in Fig. 5.

For a membrane with a jump in the mean curvature, the Fourier amplitudes a_i should decay as a function of the wave number $|\mathbf{k}^{(i)}|$ with a power law. It is shown in the Appendix that a discontinuity of the mean curvature along a line implies the asymptotic behavior

$$a_i \sim |\mathbf{k}^{(i)}|^{-7/2} \tag{7}$$

for large $k^{(i)}$. This result can be used to determine the contribution of the domain boundary to the bending energy E_b. The calculation described in the Appendix indicates that E_b should decrease as

$$E_b \sim 1/|\mathbf{k}^{(N)}|, \tag{8}$$

where $k^{(N)}$ is the length of the largest reciprocal lattice vector.

We have therefore plotted the energy — averaged over all calculated concentrations — as a function of the inverse length of the largest reciprocal lattice vector for a given set of coefficients a_i to test this hypothesis. The data are indeed consistent with a linear $1/N$ dependence. A linear extrapolation then gives a values of $E_bL/(\kappa\ell)=(1.5\pm9.0)\times10^{-5}$ (rings) and $E_bL/(\kappa\ell)=(6.5\pm9.0)\times10^{-5}$ (caplets) for the reduced curvature energy in the limit $1/N\rightarrow0$. This result is

very interesting from the point of view of differential geometry. It suggests the existence of piecewise CMC surfaces in the limit $L\lambda/\kappa \to 0$. The membranes shown in Fig. 7 would be examples of doubly periodic piecewise CMC surfaces. The surfaces we have obtained can of course be only approximations to exact piecewise CMC surfaces.

F. Phase transitions

If the membrane forms a piecewise CMC surface in the limit of zero line tension, it is only weakly deformed by sufficiently small but finite line tensions. Here, the length ℓ of the domain boundary of the piecewise CMC surface provides an upper limit for the total energy, since the energy can only decrease when the membrane shape is allowed to relax under the effect of the line tension. The weak-line-tension limit is characterized by the curvature energy being much smaller than the line energy.

Although the line tension is very small, the main contribution to the energy (1) still comes from the vicinity of the domain boundary. The phase behavior can therefore be deduced by considering the domain perimeter ℓ shown in Fig. 8. The increase of ℓ with composition for rings and the decrease for caplet lead to a phase transition between these two morphologies. This transition takes place near the point where the boundary lengths of these configurations are the same. The caplet and ring configuration at the phase transition are shown in Fig. 1 of Ref. [40]. The same mechanism leads to the phase transition between inverted caplets and inverted rings. It takes place for somewhat smaller composition ϕ.

These phase transitions are first order, since the shape of the domain boundary does not vary continuously at the transition. Also, the total surface area of the membrane jumps at the transition. However, no noticeable changes of the radius of the passage at the phase transition have been observed.

Another type of phase transition is between rings and inverted rings and also between caplets and inverted caplets. In this case the domain type is unchanged but the components exchange their locations. The component which is inside the passage migrates to the ''outer'' part of the membrane, and vice versa.

There are also phase transitions, where the components change their locations *and* the domain type changes from ringlike to capletlike (or vice versa). Such transitions take place between inverted caplets and rings and also between inverted rings and caplets. The reason for these transitions is as follows. For small domain sizes, the domain boundary is always shorter for caplet than for ring morphologies, since it may shrink to zero when $\phi \to 0$, while for rings it is bounded from below by the passage radius. For larger domains, caplets have larger ℓ because the shape of the boundary is deformed by the passage more strongly than for the ringlike domains. Thus, large ringlike and small capletlike domains are favored, which results in these transitions.

It is interesting to note that in the weak-line-tension limit, the sequence of the phase transitions and their location is *independent* of the strength of line tension.

G. Two-component membranes: Strong line tensions

In order to obtain a complete picture of the behavior of two-component membranes of complex topology, it is necessary to consider also the case of larger line tensions. As explained in Sec. IV C above, we consider the case $\lambda L/\kappa = 1$, for which the line tension is too small to promote budding, but can have a strong effect on the passage shape, e.g., on its radius. It is important to note that although the line tension is already close to its value at the budding transition, the bending energy is about two orders of magnitude smaller than the line energy, compare Figs. 11 and 12. Surprisingly, the qualitative behavior for strong line tension is similar to the weak-line-tension case; however, there are quantitative differences.

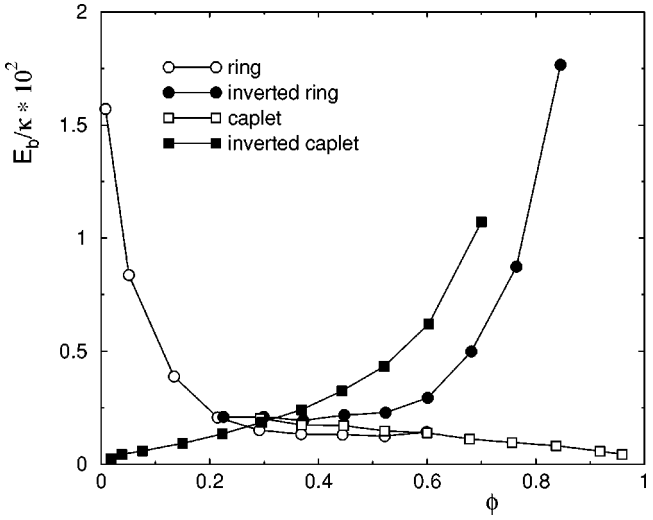

FIG. 11. Curvature energy for different morphologies as a function of composition ϕ (calculated for $N=32$ Fourier shells) in the case of large line tension. The parameters are $Lh_0^{(\alpha)}=1.2$, $Lh_0^{(\beta)}=0.4$, and $\lambda L/\kappa=1$.

The phase behavior for weak and strong line tensions is qualitatively the same. There are still three phase transitions, in order of increasing concentration between inverted caplets and rings, rings and inverted rings, and inverted rings and caplets; see Fig. 12. The phase transitions are just shifted a

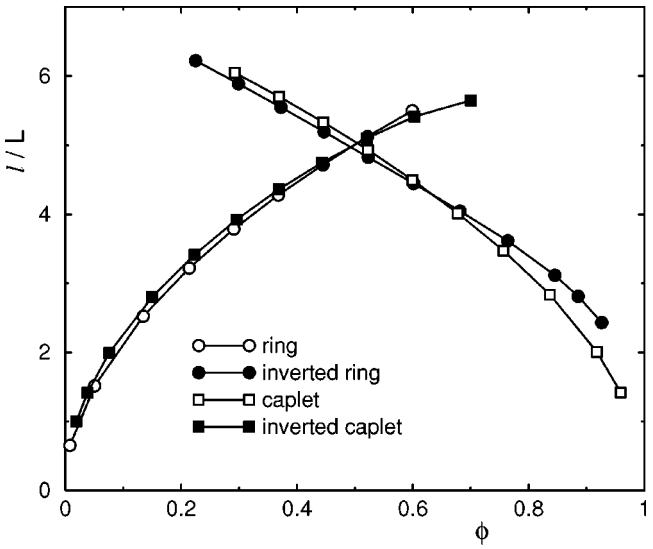

FIG. 12. Length ℓ of the domain boundaries for different morphologies as a function of composition ϕ, for the case of large line tension, $\lambda L/\kappa=1$. $N=32$ Fourier shells have been used.

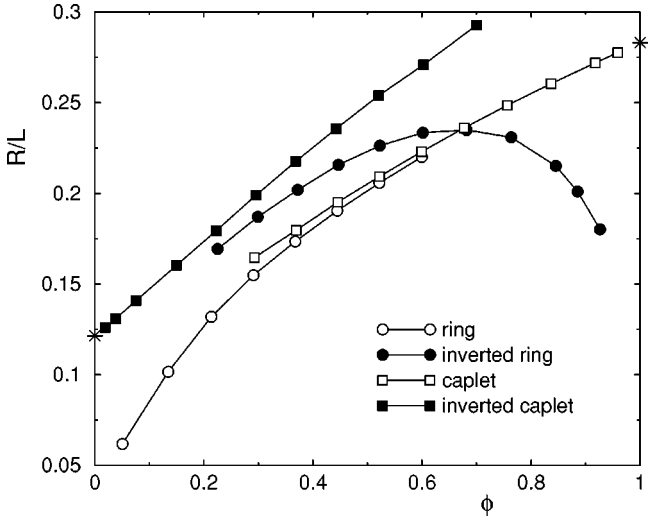

FIG. 13. Passage radius in the $z=0$ plane for different morphologies as a function of composition ϕ. The stars denote the values for pure membranes. The parameters are the same as in Fig. 11.

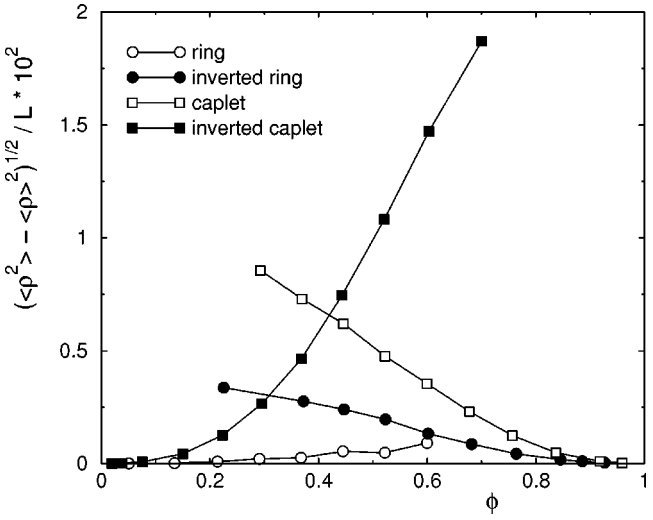

FIG. 14. Variance of the domain radius, projected into the $z=0$ plane, for different morphologies as a function of composition ϕ. The parameters are the same as in Fig. 11.

little in concentration compared to the weak-line-tension case. This is due to the decrease of the length ℓ of the domain boundaries for rings and inverted rings. The caplet morphologies are less sensitive to stronger line tension. This is intuitively understandable, since as soon as a considerable deformation of a caplet becomes favorable to decrease ℓ, formation of buds already takes over [21]. The deformation of a passage, on the other hand, costs much less bending energy, since for a given spontaneous curvature there is a whole family of CMC surfaces with different pore radii — as can be seen most easily for catenoidlike passages of zero mean curvature. Finally, we want to mention that it is easier to deform caplet-shaped domains, when the domain consists of the component with the larger spontaneous curvature.

The new feature, which appears in the case of stronger line tensions, is that for the ring and inverted ring morphologies, the passage radius no longer converges to the value of the corresponding one-component membrane in the limits $\phi\rightarrow 0$ and $\phi\rightarrow 1$, respectively. The effect of the line tension on the membrane shape is larger when the domain boundary is located closer to the center of the passage. This effect is particularly pronounced in the case of inverted rings, where the dependence of the passage radius on the concentration ϕ even becomes nonmonotonic; see Fig. 13. For $\phi>0.6$, the pore radius now *decreases* with increasing ϕ. A similar behavior is also found for the surface area.

For stronger line tensions, the shape of the domain boundary is expected to be more circular than in the weak-line-tension case, in order to minimize its length. However, the shape still deviates considerably from being circular (see Fig. 14), with larger deviations for larger domain sizes. This result should be compared with the data given in Fig. 3 of Ref. [40] for $\lambda L/\kappa=10^{-4}$; the difference is quite small. The domains of inverted configurations deviate more from circular shapes since they are more strongly influenced by the passage size, which is larger for these configurations.

V. PIECEWISE CMC VESICLES

We have shown in Sec. IV E that membranes of complex topology can form piecewise CMC surfaces in the limit of vanishing line tensions. This raises the question of whether CMC surfaces are also possible for two-component, axisymmetric vesicles of spherical topology.

It has been argued in Ref. [26] that for vesicles of fixed surface area and *zero* pressure difference between inside and outside in three dimensions, the curvature energy is not uniformly distributed on the surface — in contrast to ''vesicles'' (closed lines) in two dimensions, where the curvature distribution is uniform. However, a careful analysis of this argument shows that there is one exception: if the mean curvature is identical to the spontaneous curvature everywhere, piecewise CMC vesicles do exist in three dimensions. Since the shape and size of the vesicle are essentially determined by the spontaneous curvatures of the two components in this case, the surface area has to be considered as an unconstrained variable.

The building blocks for the construction of axisymmetric, piecewise CMC vesicles are pieces of sphere, catenoid, cylinder, unduloid, and nodoid [41]. These are the only constant-mean-curvature surfaces of rotational symmetry. The simplest example [42] of such a piecewise CMC vesicle is a cylinder of arbitrary length and radius $R_0=1/(2h_0^{(\alpha)})$, closed at the ends by hemispheres of radius $R_s=1/h_0^{(\beta)}$. Thus, a capped cylinder is only possible for the one ratio of spontaneous curvatures, $h_0^{(\beta)}/h_0^{(\alpha)}=2$, but for all compositions. Similar constructions can be made when the cylinder is replaced by an unduloid, nodoid, or catenoid. For two given spontaneous curvatures, the radius of the capping spheres is fixed to $R_s=1/h_0^{(\beta)}$. The pore radius R_0 of an unduloid or catenoid can vary from zero to $1/[2h_0^{(\alpha)}]$. In the case of *catenoid* (i.e., for $h_0^{(\alpha)}=0$) and *unduloid*, the connecting surface cannot be matched smoothly to the capping spheres if the pore is too large; this implies that the pore radius must be less than $1/h_0^{(\beta)}$. In the case of an *unduloid*, the additional condition applies that its maximum diameter $2R_1$ must be larger than the sphere diameter. Since $R_1+R_0=1/h_0^{(\alpha)}$ for unduloids [43,44], this condition implies that $0<R_0<1/h_0^{(\alpha)}-1/h_0^{(\beta)}$. An connecting unduloid is therefore only possible if $h_0^{(\beta)}>h_0^{(\alpha)}$. Finally, in the case of a *nodoid*, the

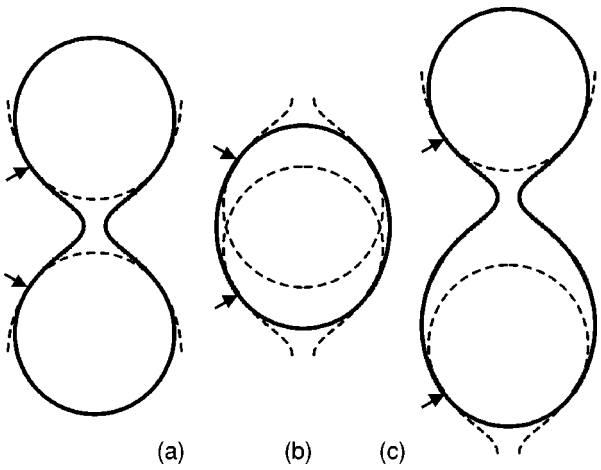

FIG. 15. Examples of piecewise constant-mean-curvature vesicles. Two spheres of the same radius $R_s=1/h_0^{(\beta)}$ are connected smoothly by an unduloid surface of mean curvature $h_0^{(\alpha)}$, with $h_0^{(\beta)}/h_0^{(\alpha)}=1.22$. (a) Small neck, (b) small caps, and (c) broken up-down symmetry. The dashed lines indicate segments of spheres and unduloids, which are not part of the vesicle surface; the domain boundary is indicated by arrows.

minimal pore radius is $R_0=1/h_0^{(\alpha)}$. Since $R_1-R_0=1/h_0^{(\alpha)}$ for nodoids [43], it is easy to show that nodoids can be connecting surfaces only for $h_0^{(\alpha)}>h_0^{(\beta)}$.

As a function of composition, the following picture emerges. For simplicity, we only consider the case of unduloids, i.e., $h_0^{(\beta)}>h_0^{(\alpha)}$. For small ϕ, two large spherical end caps are connected by a very small neck; see Fig. 15(a). With increasing pore radius, ϕ initially increases, then decreases again until a limiting shape is reached, which consists of two semispheres with a band of infinitesimal width of the second component connecting their equators. For $\phi\to 1$, there is a second class of solutions, which starts with an unduloid with very small necks, which are capped by small segments of spheres. With decreasing ϕ, the endcaps get larger; compare Fig. 15(b). Again, a limiting shape (of some finite ϕ) is reached when the pore radius approaches the sphere radius. It is clear from these arguments that in general only a limited range of compositions is accessible for such piecewise CMC vesicles with fixed spontaneous curvatures. It is worth mentioning that similar shapes occur for a fluid bridging the gap between two solid spheres in the case of complete wetting [45] and for wetting on structured substrates [46].

One can also construct more complicated piecewise CMC vesicles, for example, by breaking the up-down symmetry [see Fig. 15(c)] or by joining several surface segments of different constant mean curvature, for example sphere-unduloid-sphere-unduloid-sphere. Finally, one can imagine to construct toroidal vesicles made of several pieces of nodoids connected by pieces of spheres.

VI. SUMMARY AND CONCLUSIONS

In this paper, we have studied the behavior of multicomponent membranes of nontrivial topology within the framework of the curvature model. These membranes have the possibility of phase separation into two (or more) different phases at sufficiently low temperatures. As a result of the different, nonzero spontaneous curvatures of the components and the complex membrane topology considered, macroscopic phase separation is unfavorable. Instead, microphase separation occurs, which leads to a large variety of different domain patterns on the membrane.

The main results of our investigation are as follows. First, the shape of the membrane depends on the composition ϕ and on the type of the domain structure. While some domain morphologies lead to an almost linear dependence of the passage radius on ϕ, for example, other domain morphologies show a nonmonotonic ϕ dependence. Second, the shape of the domain boundary is strongly influenced by the topology of the membrane. For small compositions, the domains are almost circular; with increasing composition, they become increasingly noncircular in order to adjust to the passage and to the periodicity of the doubly periodic lattice. Third, the existence of smooth, doubly periodic piecewise constant-mean-curvature surfaces has been conjectured in the limit of zero line tension. We have also shown that piecewise constant-mean-curvature surfaces of spherical topology can be constructed for zero line tension. Finally, first-order phase transitions between the caplet, ring, inverted caplet, and inverted ring morphologies have been found. Here, the ring and caplet configurations dominate the phase diagram for the spontaneous curvatures employed in our calculation.

It is tempting to speculate that the mechanism of regulating the size of passages by changing the composition of a membrane may be used in cells or cell organelles [34]. A possible application of two-component membranes could be the crystallization of membrane proteins in CMC surfaces [47], where the enrichment of one component near the protein provides an extra degree of freedom for optimal hydrophobic matching [48,49,8].

ACKNOWLEDGMENTS

We thank J. Goos for providing the first version of the program for minimizing the curvature energy of a lattice of passages. Helpful discussions with D. Andelman, W. Fenzl, J. Goos, T. Kawakatsu, P. Lenz, R. Lipowsky, U. Schwarz, and M. Wortis are also gratefully acknowledged.

APPENDIX: FOURIER SERIES OF A FUNCTION WITH DISCONTINUOUS SECOND DERIVATIVE

For a scalar function $f(x)$ in *one* dimension with a jump in its second derivative, its Fourier transform $f(q)$ decays as $f(q)\sim q^{-3}$ for large q. For a scalar function $f(\mathbf{r})$ in *two* dimensions, which is rotationally symmetric and has a jump in its second derivative along a circle around the origin, the Fourier transform reads

$$f(q)=2\pi\int dr\, r f(r) J_0(qr), \tag{A1}$$

where $J_0(x)$ is a Bessel function of first kind. In the limit of large x, $J_0(x)=\sqrt{2/\pi x}[\cos(x-\pi/4)+O(1/x)]$, so that

$$f(q) \simeq 2\sqrt{\frac{2\pi}{q}} \int dr \sqrt{r} f(r) \cos(qr - \pi/4) \qquad \text{(A2)}$$

for large q. The integral behaves like the one-dimensional Fourier transform of a function with a discontinuity in its second derivative, and therefore decays as q^{-3}. Thus, we finally obtain

$$f(q) \sim q^{-7/2}. \qquad \text{(A3)}$$

This result can now be used to estimate the dependence of the curvature energy on the largest wave vector Λ. Consider an almost planar membrane in the Monge parametrization, $z = f(\mathbf{r})$, with a discontinuity of the spontaneous curvature along a circle. The curvature energy reads in this case

$$E_b \sim \kappa \int d^2q [q^2 f(q) - H_0(q)]^2. \qquad \text{(A4)}$$

For a finite number N of wave vectors, we assume $f(q)$ to be the same as in the limit $N \to \infty$ for $q < \Lambda$, but $f(q) = 0$ for $q > \Lambda$. Then, the curvature energy becomes

$$E_b \sim \kappa \int_{q>\Lambda} d^2q H_0(q)^2 \sim \kappa \int_{\Lambda}^{\infty} dq\, q\, q^4\, q^{-7} \sim \Lambda^{-1}. \qquad \text{(A5)}$$

[1] M. Bloom, E. Evans, and O. G. Mouritsen, Q. Rev. Biophys. **24**, 293 (1991).
[2] *Handbook of Biological Physics*, edited by R. Lipowsky and E. Sackmann (Elsevier, Amsterdam, 1995), Vols. 1A and 1B.
[3] R. B. Gennis, *Biomembranes: Molecular Structure and Function* (Springer-Verlag, New York, 1989).
[4] E. Sackmann, in *Handbook of Biological Physics*, edited by R. Lipowsky and E. Sackmann (Elsevier, Amsterdam, 1995), Vol. 1A, pp. 1–63.
[5] S. Subramaniam and H. M. McConnell, J. Phys. Chem. **91**, 1715 (1987).
[6] P. A. Rice and H. M. McConnell, Proc. Natl. Acad. Sci. USA **86**, 6445 (1989).
[7] C. L. Hirschfeld and M. Seul, J. Phys. (France) **51**, 1537 (1990).
[8] M. Edidin, Curr. Opin. Struct. Biol. **7**, 528 (1997).
[9] O. G. Mouritsen and K. Jørgensen, Curr. Opin. Struct. Biol. **7**, 518 (1997).
[10] S. H. Wu and H. M. McConnell, Biochemistry **14**, 847 (1975).
[11] C. Gebhardt, H. Gruler, and E. Sackmann, Z. Naturforsch. C **32**, 581 (1977).
[12] M. R. Vist and J. H. Davis, Biochemistry **29**, 451 (1990).
[13] J. L. Thewalt and M. Bloom, Biophys. J. **63**, 1176 (1992).
[14] A. K. Hinderliter, J. Huang, and G. W. Feigenson, Biophys. J. **67**, 1906 (1994).
[15] M. Bloom and O. Mouritsen, in *Handbook of Biological Physics*, edited by R. Lipowsky and E. Sackmann (Elsevier, Amsterdam, 1995), Vol. 1A, pp. 65–95.
[16] N. Dan, P. Pincus, and S. A. Safran, Langmuir **9**, 2768 (1993).
[17] R. R. Netz and P. Pincus, Phys. Rev. E **52**, 4114 (1995).
[18] D. D. Lasic and D. Papahadjopoulos, Science **267**, 1275 (1995).
[19] H. E. Warriner, S. H. J. Idziak, N. L. Slack, P. Davidson, and C. R. Safinya, Science **271**, 969 (1996).
[20] S. Leibler and D. Andelman, J. Phys. (France) **48**, 2013 (1987).
[21] R. Lipowsky, Biophys. J. **64**, 1133 (1993).
[22] J. L. Harden and F. C. MacKintosh, Europhys. Lett. **28**, 495 (1994).
[23] F. Jülicher and R. Lipowsky, Phys. Rev. Lett. **70**, 2964 (1993).
[24] F. Jülicher and R. Lipowsky, Phys. Rev. E **53**, 2670 (1996).
[25] D. Andelman, T. Kawakatsu, and K. Kawasaki, Europhys. Lett. **19**, 57 (1992).
[26] T. Kawakatsu, D. Andelman, K. Kawasaki, and T. Taniguchi, J. Phys. II **3**, 971 (1993).
[27] T. Taniguchi, K. Kawasaki, D. Andelman, and T. Kawakatsu, J. Phys. II **4**, 1333 (1994).
[28] T. Hashimoto, S. Koizumi, H. Hasegawa, T. Izumitani, and S. T. Hyde, Macromolecules **25**, 1433 (1992).
[29] I. W. Hamley *et al.*, Macromolecules **26**, 5959 (1993).
[30] D. A. Hajduk *et al.*, Macromolecules **30**, 3788 (1997).
[31] W. Harbich, R. M. Servuss, and W. Helfrich, Z. Naturforsch. A **33**, 1013 (1978).
[32] X. Michalet, D. Bensimon, and B. Fourcade, Phys. Rev. Lett. **72**, 168 (1994).
[33] P. K. J. Kinnunen, Chem. Phys. Lipids **57**, 375 (1991).
[34] B. Alberts *et al.*, *Molecular Biology of the Cell*, 2nd ed. (Garland, New York, 1989).
[35] H. B. Lawson, Ann. Math. **92**, 335 (1970).
[36] The case of a square or hexagonal lattice has only been considered approximately in Ref. [22], where the unit cell has been replaced by a circular disk of equal area.
[37] No stronger singularity of the mean curvature than a discontinuity can occur, because the curvature energy would otherwise diverge.
[38] S. T. Hyde, J. Phys. (Paris), Colloq. **51**, C7-209 (1990).
[39] D. M. Anderson, H. T. Davis, L. E. Scriven, and J. C. C. Nitsche, Adv. Chem. Phys. **77**, 337 (1990).
[40] W. T. Góźdź and G. Gompper, Phys. Rev. Lett. **80**, 4213 (1998).
[41] M. Giaquinta and S. Hildebrandt, *Calculus of Vaiations I* (Springer-Verlag, Berlin, 1996).
[42] M. Wortis (private communication).
[43] P. Lenz, Ph.D. thesis, Universität Potsdam, 1998.
[44] This result follows from an integration of the mean curvature, given by Eq. (4), over a projected area which is bounded by circular rings of minimum and maximum radii, R_0 and R_1, respectively. The evaluation of this integral, which equals $\pi(R_1^2 - R_0^2) H_0^{(\alpha)}$, with the use of the Gauss divergence theorem immediately provides the desired relation.

[45] D. M. Smith and N. E. Olague, J. Phys. Chem. **91**, 4066 (1987).
[46] P. Lenz and R. Lipowsky (unpublished).
[47] E. Pebay-Peyroula, G. Rummel, J. P. Rosenbusch, and E. M. Landau, Science **277**, 1676 (1997).
[48] O. G. Mouritsen and M. Bloom, Biophys. J. **46**, 141 (1984).
[49] F. Dumas, M. M. Sperotto, C. Lebrun, J.-F. Tocanne, and O. G. Mouritsen, Biophys. J. **73**, 1940 (1997).